POLYPUBLIE
Polytechnique Montréal

POLYTECHNIQUE MONTRÉAL
UNIVERSITÉ D'INGÉNIERIE

Titre: Title:	Anti-stokes fluorescence cooling of lanthanum aluminosilicate glasses
Auteurs: Authors:	Thomas Meyneng, Malek Aïssaoui, Nicolas Grégoire, Philippe Labranche, Steeve Morency, Jean-Sébastien Boisvert, Vladimir Karpov, Younès Messaddeq, & Raman Kashyap
Date:	2025
Type:	Article de revue / Article
Référence: Citation:	Meyneng, T., Aïssaoui, M., Grégoire, N., Labranche, P., Morency, S., Boisvert, J.-S., Karpov, V., Messaddeq, Y., & Kashyap, R. (2025). Anti-stokes fluorescence cooling of lanthanum aluminosilicate glasses. Optical Materials Express, 15(4), 724-736. https://doi.org/10.1364/ome.557988

Document en libre accès dans PolyPublie
Open Access document in PolyPublie

Document publié chez l'éditeur officiel
Document issued by the official publisher

Anti-Stokes fluorescence cooling of lanthanum aluminosilicate glasses

T. Meyneng,[1,2,*] [iD] **M. Aïssaoui,[2] N. Grégoire,[1] P. Labranche,[1] S. Morency,[1] J. S. Boisvert,[2] V. Karpov,[3] Y. Messaddeq,[1] and R. Kashyap[2,4]**

[1]*Centre d'optique photonique et laser, Université Laval, Québec G1V A06, Canada*
[2]*Département de génie électrique, École polytechnique de Montréal, Montréal H3T 1J4, Canada*
[3]*MPB Communication, 147 Hymus Blvd, Pointe-Claire, Canada*
[4]*Département de génie physique, École polytechnique de Montréal, Montréal H3T 1J4, Canada*
*thomas.meyneng.1@ulaval.ca

Abstract: This study reports on the fabrication of ytterbium-doped lanthanum-aluminosilicate (LAS) glasses using the modified chemical vapor deposition (MCVD) process combined with solution doping. The fabricated samples exhibit near-unity quantum efficiencies and background absorptions below 10 dB·km^{-1}, enabling the observation of anti-Stokes fluorescence cooling (ASFC) under excitation wavelengths ranging from 1030 to 1080 nm. Measurements conducted in ambient conditions demonstrated net cooling of up to −8.2 K from room temperature in small bulk samples and −7.9 K in long rods of the material.

1. Introduction

For nearly three decades, anti-Stokes fluorescence cooling (ASFC) has served as a reliable technique to achieve non-contact refrigeration in solid-state materials [1]. A significant proportion of the results have been achieved using ytterbium-doped (Yb) materials. Trivalent ytterbium ions exhibit low quantum defects transition and a simple energy level structure, enabling near unitary quantum efficiencies necessary for net cooling [2]. However, stringent requirements are imposed on the host material, which must minimize parasitic heating mechanisms effectively. These arise primarily from multiphonon decay, concentration quenching, and background absorption due to impurities [3]. Consequently, over the years, a limited variety of materials have been able to demonstrate Yb-ASFC. Fluorides remain one of the most successful materials, because of their high rare-earth solubility and low phonon energies. Fluorozirconates glass were the first hosts sufficiently optimized to demonstrate ASFC [1] and served as an useful platform to understand and improve techniques around the effect. Results in ZBLAN rapidly scaled to demonstrate up to 65 K of net cooling, starting from room temperature [4]. Today, it still receives interest, in the form of fiber [5,6], as research is moving toward the application of ASFC with radiation-balanced fiber lasers. Fluoride single crystal, mostly the scheelite YLiF$_4$ phase, breached the cryogenic point (123 K) and established cooling records, which are still in place to this day [7].

In 2020, the demonstration of ASFC in silicate fibers [8] and then in bulk [9] opened new possibilities. Silica, one of the gold standards of photonic, found another field to establish itself. The following years, Knall et al. demonstrated the first radiation-balanced silicate fiber laser [10]. Since then, the net cooling values achieved surpassed what was observed in ZBLAN [11], and the results of the radiation-balanced fiber laser have been scaled up to 200 mW [12]. The technological maturity surrounding silica fiber fabrication fulfills the stringent purity requirement necessary for ASFC. One part of the research effort aims to extend the limit of doping concentration, by developing new glass compositions [13,14] and/or alternative doping methods, compatible with vapor deposition techniques [15]. Our interest was directed at the $REE_2O_3 - Al_2O_3 - SiO_2$ system, with ($REE = Y/Gd/La/Lu$). These glass compositions started

to receive attention in the late 1980s [16,17]. Incorporation of REE_2O_3 as a modifier leads to a marked increase in both the glass density and the refractive index. The elevated concentration of rare earth elements in the glass network enhances the solubility of lanthanides [18,19] and correlates to decreased multiphonon relaxation rates [13,20]. Improved photodarkening resistance was also observed [21] but associated with the high Al_2O_3 concentration. As these studies revolved around the use of melt-quenching approaches, they are limited to an upper limit of melting temperature. Our work present the use of MCVD - Solution doping to fabricate such glass compositions, accessing the high SiO_2 fraction domain of the $La_2O_3 - Al_2O_3 - SiO_2$ (LAS) ternary diagram. We demonstrate the fabrication of Yb-LAS glasses with concentrations reaching 10^{26} ions $\cdot$ m^{-3}, maintaining a near-unitary quantum efficiency with background absorption of less than 10 dB $\cdot$ km^{-1}. Small bulk samples were cooled by up to -8.2 K from room temperature under ambient conditions, using a 18W - 1035 nm pump. A 25 cm rod was cooled by up to -7.9 K from room temperature using a 1070 nm, 227 W pump.

2. Materials and methods

2.1. Sample fabrication

The glass samples were derived from preforms fabricated using the standard Modified Chemical Vapor Deposition (MCVD) solution doping technique. Silica soot was deposited on a Heraeus F300 silica tube at temperatures ranging from 1320 °C to 1350 °C. In parallel, aqueous solutions of the element of interest were prepared, from the dissolution of aluminum chloride hexahydrate ($AlCl_3.6H_2O$), lanthanum chloride heptahydrate ($LaCl_3.7H_2O$) and ytterbium chloride hexahydrate ($YbCl_3.6H_2O$), in 250 mL of analytical grade water. The chloride salt purity is 99.9999%w, provided by PureAnalytical. The soot was soaked with the solution for a duration of 15 minutes and dried under N_2 gas for 6 hours. The tube is then reinstalled on the MCVD lathe and dried thermally / chemically from 400 to 1150°C, under He, O_2 and Cl_2. The vitrification of the soot is carried out in a two-step process at 1600 °C and subsequently at 2000 °C. Finally, the preform is collapsed at 2150 °C. The bulk glass samples were extracted directly from the preform and mechanically polished to remove most of the silica cladding, resulting in final dimensions of $12 \times 1.8 \times 1.8$ mm. For the rod sample, the preform was etched in hydrofluoric acid from 15 to 7 mm and drawn into 3.5 mm diameter rods. A final etching step brought the outside diameter to 2 mm, with a core diameter of 750 microns. A 25 cm section was extracted and polished on both faces. The nomenclature used for the sample is referred to as GLaA X/Y. The X and Y values indicate the fraction of Lanthanum (X) to Ytterbium (Y) used in the solution. The three samples presented in this study—GLaA Undoped, GLaA 90/10, and GLaA 75/25—contain 0, 0.37, and 0.85 cationic percent of Ytterbium, respectively.

2.2. Elemental analysis

The elemental composition of polished cross sections of the preform cores were analyzed using a Cameca SX100 electron microprobe operating at an accelerating voltage of 15 kV. Elemental line scans were performed over a 2000 μm length at 50 μm intervals, with a total acquisition time of 30 minutes.

2.3. Refractive index measurement

The refractive index profile of the preform core was obtained using a photon kinetics PK2660 device, at a wavelength of 632.2 nm.

2.4. Density measurement

The density of all samples was determined using the Archimedes method. The sample cladding was mechanically removed, leaving only the core glass. The measurements were carried out

using deionized water as the immersion liquid at 21 °C. Each measurement was performed 10 times, and the average value was calculated.

2.5. Absorption coefficient measurement

The absorption coefficient data were obtained from bulk transmission from 850 to 1030 nm, using two 1 mm and 10 mm polished preform slices. Transmission data were recorded from 200 to 1500 nm on an Agilent Carry 5000 spectrometer, using a 1 nm step size and 1 second acquisition time, using a sample carrier with 1.5 mm diameter pinhole, to match the size of the core of the preform.

The absorption coefficient data from 1030 to 1080 nm were made from the power absorption on 25 cm rods of samples, using a 1030-1080 nm tunable laser (YFL-20, 20 watt fiber from MPB Communication) below 200 mW output power. The absorption coefficient was recalculated from the following relation considering normal incidence conditions.

$$\alpha(\lambda) = \frac{-1}{t} ln(\frac{P_{out}(1 + R_f)}{P_{in}(1 - R_f)}) \tag{1}$$

With t the sample thickness, P_{in} and P_{out} respectively the laser input and output power and R_f the Fresnel reflection, calculated at 1030 nm, with $n_{sample} = 1.4861$.

2.6. Cross section calculations

The absorption cross-sectional data were obtained from the absorption coefficient data of the GLaA 75/25 sample and the Yb-ion density N_{Yb}

$$\sigma_{absorption}(\lambda) = \frac{\alpha(\lambda)}{N_{Yb}} \tag{2}$$

The emission cross-section data was calculated from the Füchtbauer–Ladenburg relation:

$$\sigma_{emission}(\lambda) = \frac{\lambda^5}{8\pi cn^2\tau_r} \frac{I(\lambda)}{\int I(\lambda)d\lambda} \tag{3}$$

where λ is the emission wavelength, c the speed of light in vacuum, n the refractive index of the core glass, τ_r the radiative lifetime. $I(\lambda)$ was obtained from the normalized emission spectra of sample GLaA 75/25.

2.7. Quantum efficiency measurement

The tunable YFL-20 laser, operating in the 1030–1080 nm range, was employed to measure the photoluminescence (PL) emission spectra. The emitted light was collected using an integrating sphere, which was coupled to a multimode optical fiber and directed to an optical spectrum analyzer (OSA), Yokogawa AQ6370E, with a working range of 600–1700 nm. The external quantum yield (η_{EQE}) is defined as the ratio of the number of photons emitted to the number of photons absorbed.

$$\eta_{EQE} = \frac{N_{ep} - (1 - A)N_{epd}}{N_{ip}A} \tag{4}$$

where N_{ep} is the number of photons emitted by the sample when it is placed inside the integrating sphere and the pump beam is directed onto the sample, N_{ip} is the number of incident photons when the pump laser beam is directed toward the sphere without the sample, and N_{epd} is the number of photons emitted by the sample when it is inside the integrating sphere and the excitation laser beam is directed onto the sphere wall, from its interaction with the diffused light.

2.8. Background absorption measurement

Background absorption values were obtained from the attenuation of fibers from the GLaA sample. After MCVD fabrication, 15 cm of the preforms were set aside for drawing, while another section was dedicated to the bulk/rod transformation. The three GLaA preforms (i.e., undoped, 90/10, and 75/25) were drawn into 125-micron fibers, resulting in a core diameter of 11 microns. A broadband supercontinuum source, spanning 500–2400 nm, was injected into a 500-meter spool of fiber. The fiber's output end was spliced to a 105/125-micron multimode fiber and connected to a Yokogawa AQ6370E OSA, which recorded data from 600–1700 nm. Three successive cutbacks of 490 meters, 5 meters, and 1 meter were performed to obtain the attenuation spectra.

2.9. Mean fluorescence wavelength calculation

The mean fluorescence wavelength (MFWL) of the sample was determined from its emission spectra, obtained via side-emission measurements under excitation at 1030 nm with an input power of 120 mW. Luminescence was collected using a multimode fiber with a core diameter of 200 μm, which was coupled to an optical spectrum analyzer (OSA). The spectra were recorded at room temperature, and the MFWL (λ_{MFWL}) was calculated using the following equation:

$$\lambda_{MFWL} = \frac{\int \lambda S(\lambda) d\lambda}{\int S(\lambda) d\lambda} \tag{5}$$

With λ the wavelength and $S(\lambda)$ the spectral density of the emitted spectra.

## 2.10. Anti-Stokes fluorescence cooling measurement

2.10.1. Thermal camera calibration

Figure 1 illustrates the calibration procedure for the SC645 thermal camera used in the ASFC measurement. A silica plate, extracted from an F300 tube, was chosen as the calibration reference since it constitutes the outer material of all samples. The setup incorporates a Peltier TEC cell in contact with a copper plate. The silica sample is placed on the copper plate, and thermal paste is applied at the junction to enhance thermal contact. The device operates within a range of −35°C to +35°C relative to room temperature; however, measurements were conducted between 5°C and 40°C to avoid water condensation at sub-zero temperature. The thermal camera was focused at the same working distance (0.5 m) as the standard measurement, and a thermocouple was placed on the silica plate. Temperature scans were applied to the silica plate. An emissivity of 0.82 was selected as it resulted in the smallest difference between the thermal camera and thermocouple readings.

2.10.2. Bulk measurements

The ASFC measurements were performed using the YFL-20 1030-1080 nm fiber laser, at a constant power of 18 watt. The samples were placed in an aluminum chamber, coated with absorbent paint on the inside. A 75 mm focal length lens with antireflective coating (650-1050 nm), was placed at 45 mm of the sample. For single-pass measurements, the beam was collected in a beam dump, placed outside the thermal camera field of view. For double pass measurement, the output beam was collected and collimated using a 30 mm focal lens, with an antireflective coating (650-1050 nm) and reinjected onto the sample with a flat mirror, with dielectric coating (99.5% from 700 to 1100 nm).

Dynamic temperature measurements were performed using a FLIR SC645 thermal camera. The recordings were performed using a sample emissivity of 0.82, for a sample-to-camera distance of 0.5 meters. The ambient room temperature was measured to be between 21.2 and
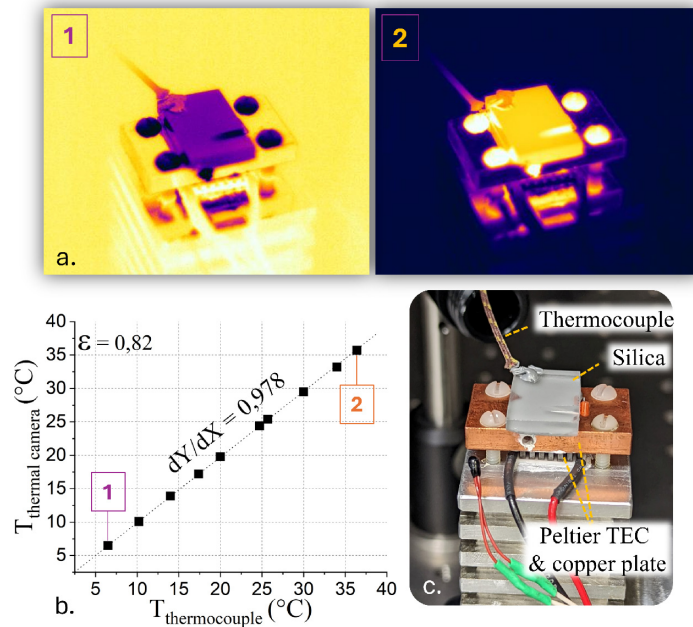
Fig. 1. a. Thermal images of the TEC heated/cooled silica plate **b.** temperature readings from the thermocouple (x-axis) and the thermal camera (y-axis), for an emissivity of 0.82 **c.** photograph of the calibration setup

21.6 °C with humidity ranging from 40 to 50%. The recordings were performed at 6 image per second. The laser was blocked for the first 30 seconds of measurement. The shutter was then open for 4 minutes to reach steady state conditions. Each successive recording was spaced from 10 to 15 minutes to allow the chamber and optics to cool. The data is displayed as $\Delta T = T_{sample} - T_{sample-LaserOFF}$, with $T_{sample-LaserOFF}$ calculated from an average of the first 25 seconds of recording. In the single-pass configuration, we present the sample temperature at the laser entrance and the output, since a thermal gradient is always present, even for a 1 cm long sample. The temperature of each face was determined by an average of the first and last 3 mm of the sample. For the double-pass configuration, the thermal gradient was reduced by pump reinjection and the sample temperature was obtained from an average throughout the length.

2.10.3. Rod measurements

The ASFC rods measurements were made using a 25 cm rod of the GLaA 75/25 preform. The core glass presents diameters of 0.75 mm, with a surrounding cladding of 2 mm. The rod was placed on homemade quartz holders. The rod was pumped with a YLR-300-AC laser, from IPG Photonics, operating at 1070±5 nm, up to a power of 227 W. An enclosed optical table was used for the optical setup to reduce convection effects caused by the room's ventilation.

3. Results

3.1. Sample properties

The results presented in this section analyze three different lanthanum-aluminosilicate glasses, including two ytterbium-doped samples and one pristine sample, which serves as a reference. The ionic density and other relevant properties are summarized in Table 1. Figure 2 illustrates (a) photographs of the polished samples, (b) an SEM image of a polished cross-section slice of

GLaA 75/25 preform, and (c) the corresponding elemental analysis profile obtained via EPMA analysis.
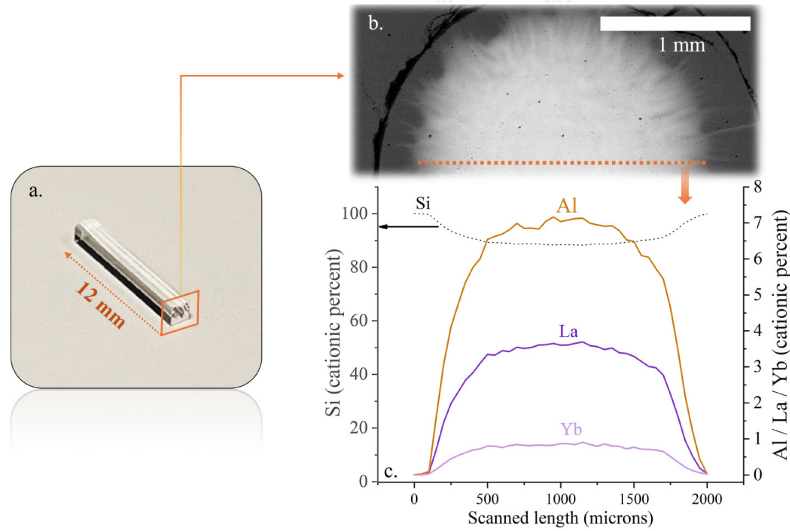

Fig. 2. a. From left to right - GLaA 90/10, GLaA 75/25 and GLaA 75/25 Brewster Cut samples b. SEM-BSE image of GLaA 75/25 c. Elemental analysis profile of GLaA 75/25, plotted from EPMA measurment

Table 1. Properties of GLaA samples

Sample Name	N_{Yb} (ions.m^{-3})	η_{EQE}	$\alpha_{background}$ (dB.km^{--1})	λ_{MFWL} (nm)	Lifetime (*ms*)	Core composition Al / La / Yb ($\%_{cationic}$)
GLaA - Undoped	-	-	8.01 $_{(1030nm)}$	-	-	7.21 / 4.32 / -
GLaA - 90/10	$4.3\ 10^{25}$	0.989	10.41 $_{(1200nm)}$	1004.4	0.85	7.13 / 4.23 / 0.37
GLaA - 75/25	$1.26\ 10^{26}$	0.985	9.80 $_{(1200nm)}$	1004.6	0.87	7.09 / 3.62 / 0.85

The sample core, which contains the LAS glass, has a diameter of 1.65 millimeters. The glass composition at the core center is comprised of 7.2 cationic percent ($\%_{cationic}$) of aluminum (Al) and 4.3 $\%_{cationic}$ of lanthanum (La). The ytterbium was added in substitution of the lanthanum, to maintain the total rare-earth concentration (La + Yb) similar for all samples. The doped sample, namely GLaA - 90/10 and GLaA - 75/25 respectively present 0.37 and 0.85 $\%_{cationic}$ of Yb. The high level of codopant significantly increases the glass density to 2.28 ± 0.02 g/cm^3. A similar trend is also reflected on the core refractive index, which exhibits a positive contrast of 2.9×10^{-2} to 3.2×10^{-2} compared to the silica cladding, at 632 nm. Consequently, the glass demonstrates a numerical aperture of 0.3. The core-cladding interface is blurred by chemical diffusion effect, and stria are visible, originating from inhomogeneous mixing during the preform collapse. However, the presence of these defects still results in attenuation values close to or below 10 dB.km^{-1} in a fiber form, their attenuation profile are displayed in Fig. 4. The undoped fiber provided background attenuation of 8.01 dB.km^{-1} at 1030 nm. All fiber samples showed similar OH absorption at 1380 nm, averaging 23 dB.km^{-1}, resulting from an aggressive chlorine drying during fabrication. The removal of the Cl$_2$ flow during processing usually results in fiber showing 150 to 200 dB.km^{-1} absorptions at 1380 nm. The GLaA-Undoped attenuation curve demonstrate residual Yb-absorption, due to residues present in the solution-doping kit used for the fabrication.

Table 1 presents the ion density, quantum efficiency, background absorptions, and mean fluorescence wavelength (MFWL) values of the GLaA samples. The doped samples present near unity quantum efficiency values. The MFWL values of both samples are quasi-similar, at 1004.4 and 1004.6 nm, unaffected by the difference in doping concentration. The absorption spectra of both doped samples are displayed in Fig. 3(a). At 976 nm, the GLaA 90/10 sample presents an absorption coefficient value of 1.23 cm^{-1}, while the GLaA 75/25 shows 3.83 cm^{-1}. The absorption and emission cross sections were calculated from absorption spectra and emission measurement and are shown in Fig. 3(b).
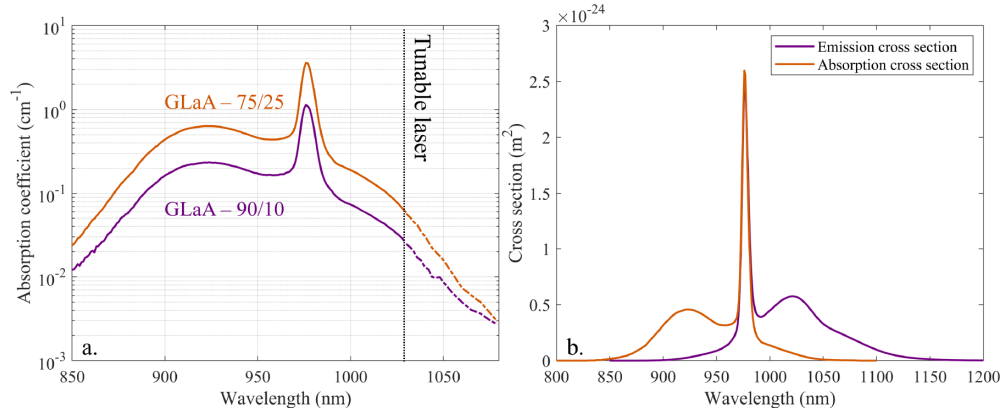
Fig. 3. a. Absorption coefficient of samples, data from 1030 - 1080 nm were obtained using the power absorption method, with the tunable laser. b. Absorption and emission cross section of sample GLaA 75/25
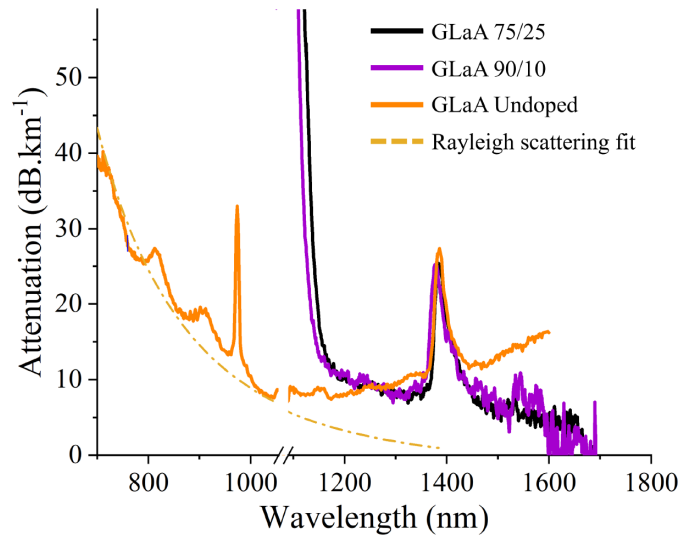

Fig. 4. Attenuation profile of the LAS sample, drawn in 11/125 microns fiber.

3.2. Anti-Stokes fluorescence cooling measurement

3.2.1. Bulk samples

Figure 5 illustrates the dynamic temperature evolution of bulk samples with dimensions of 12 × 1.8 × 1.8 mm, pumped at a wavelength of 1030 nm with a power of 18 W in a single-pass configuration. The results are presented as the temperature change (ΔT) relative to room temperature. Given the temperature gradient observed along the length of the doped samples, separate temperature measurements are provided for the laser entrance and exit points. The figure includes data for three samples from the GLaA series, along with a reference sample of pure silica extracted from a high-purity Heraeus F300 tube. The undoped GLaA and F300 samples serve as benchmarks to account for parasitic heating under the specified pumping conditions. The undoped GLaA sample exhibits a temperature increase of 1.2 K after 175 seconds of pumping. The observed decrease in temperature following pump shutdown confirms that the heating was induced by the laser. The F300 sample shows a temperature increase of 0.1 K, which is close to the detection limit of the thermal camera. In contrast, the doped samples exhibit distinct cooling effects. The GLaA 90/10 sample demonstrates a temperature reduction of −1.9 K at the laser entrance and −1.4 K at the exit after 175 seconds. Similarly, the GLaA 75/25 sample shows cooling of up to −5.5 K at the laser entrance and −4.8 K at the exit.
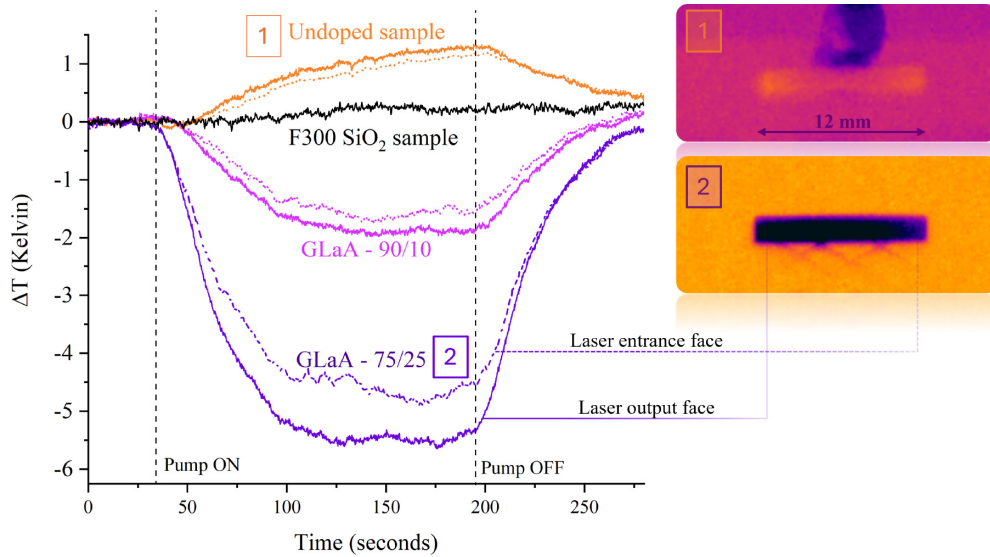

Fig. 5. Dynamic temperature evolution of samples, under 1030 nm / 18W pumping, in a single pass configuration. The inset images shows the thermal image recorded at t = 150 seconds.

The doped samples were also tested in double-pass configuration, by re-injecting the residual pump power with a high-reflectivity dielectric mirror. In addition, the pump wavelength was varied from 1030 to 1040 nm, with a fixed power of 18W, to identify the optimal excitation wavelength. The results are shown in Fig. 6. Theoretical ΔT was calculated using the relation.

$$C\frac{dT}{dt} = -P_{ASFC} + P_{surr} \tag{6}$$

With C the specific heat, P_{ASFC} the cooling power, equal to the ASFC efficiency, multiplied by the absorbed pump power $\eta_{cool}P_{abs}$. P_{surr} corresponds to the heating load of the surrounding environment, which in our measurement conditions is the radiative heat load and the convective
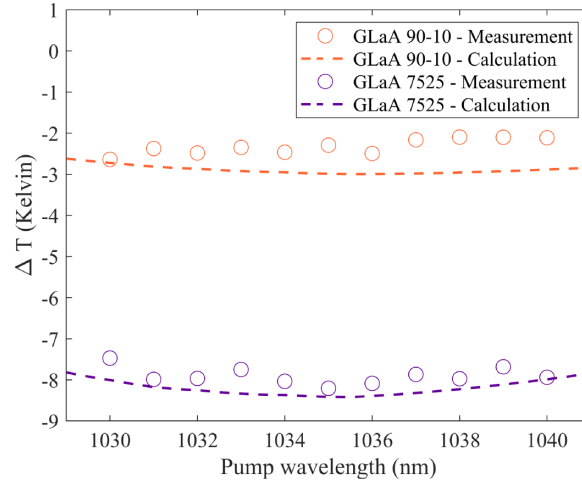
Fig. 6. Maximum net cooling obtained for GLaA 90/10 and GLaA 75/25, in a double pass configuration, with a pump wavelength varying from 1030 to 1040 nm, with a fixed power of 18W. The dashed line displays theoretical calculations, obtained from samples properties

heat load. Taken in steady-states, the relation becomes:

$$\eta_{cool}P_{abs} = \Delta T(4\epsilon S_{sample}\sigma_B T_{RT}^3 + \kappa_{conv}S_{sample}) \tag{7}$$

ϵ correspond to the emissivity of the sample, fixed at a value of 0.82, S_{sample} the surface area of the sample, σ_B the Stefan–Boltzmann constant, T_{RT} the room temperature (294.15 Kelvin), κ_{conv} is the coefficient heat-transfer coefficient, with $\kappa_{conv} = 18.65 W.m^{-2}.K^{-1}$ as in Ref. [22]. In the double-pass configuration, we consider the absorbed pump power equal to :

$$P_{abs} = P_{in}(1 - R_{fresnel})(1 - e^{-\alpha(\lambda,T)l})(1 + T_{lens}^2 R_{mirror}e^{-\alpha(\lambda,T)l}) \tag{8}$$

With $R_{fresnel}$ the Fresnel reflection, lost at the sample entrance, $\alpha(\lambda, T)$ the sample absorption coefficient at the pump wavelength, T_{lens} the transmission of the lens in the reinjection system (99.2%), R_{mirror} the mirror reflectivity, and l the length of the sample.

η_{cool} is defined as

$$\eta_{cool} = \eta_{abs}\eta_{EQE}(\frac{\lambda_{MFWL}}{\lambda_{pump}}) - 1 \tag{9}$$

With λ_{MFWL} the mean fluorescence wavelength, λ_{pump} the pump wavelength and η_{abs} the absorption efficiency :

$$\eta_{abs} = \frac{\alpha(\lambda, T)}{\alpha(\lambda, T) + \alpha_{parasitic}} \tag{10}$$

For the theoretical calculations of ΔT, the temperature dependence of the absorption coefficient was not taken into account, as the temperature variations in the sample were relatively small.

The results of the double-pass experiments (circles) and the calculation results (dotted line) are provided in Fig. 6. Compared to the single-pass setup, cooling values have increased in both doped samples. Sample GLaA 90/10 demonstrated the highest cooling at 1030 nm excitation, at −2.7K, sample GLaA 75/25 reached −8.2K of cooling at 1035 nm. The temporal evolution of the temperature was fitted to an exponential decay fit, in a procedure similar to Topper et al. [23] using $\Delta T(t) = \Delta T_{max}(1 - e^{-t/\tau})$. The samples GLaA 90/10 and GLaA 75/25 exhibited τ values of 53.8 seconds and 26.4 seconds, respectively. The calculations indicate a slight overestimation of ΔT_{max}, which may be attributed to the absorption coefficient not being adjusted for thermal

variations. For the GLaA 75/25 sample, the experimentally determined optimal pump wavelength (OPWl) aligns well with the calculated value, both falling at 1035 nm. In contrast, the GLaA 90/10 sample shows a discrepancy between experimental and calculated OPWl. Although the experimental data indicate a minimum at 1030 nm, the calculations predict an optimal wavelength at 1034 nm.

3.2.2. Rod sample

This section presents the results obtained for a 25 cm rod of the GLaA 75/25 sample, pumped using a high-power Yb laser operating at 1070 nm. The diameter of the rod core was reduced to 750 microns, for a total diameter of 2 mm considering the residual silica cladding. Figure 7 includes photographs of the sample and the experimental setup used for the measurements.
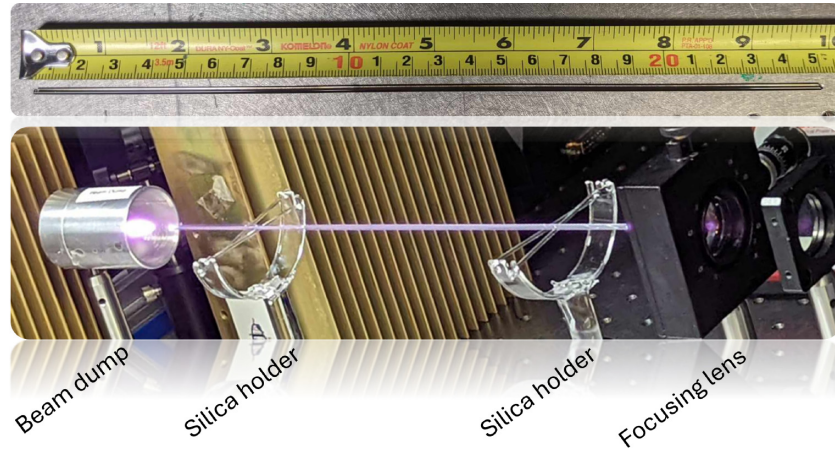
Fig. 7. Photos of the GLaA 75/25 rod, and the ASFC setup, with the pumped rod
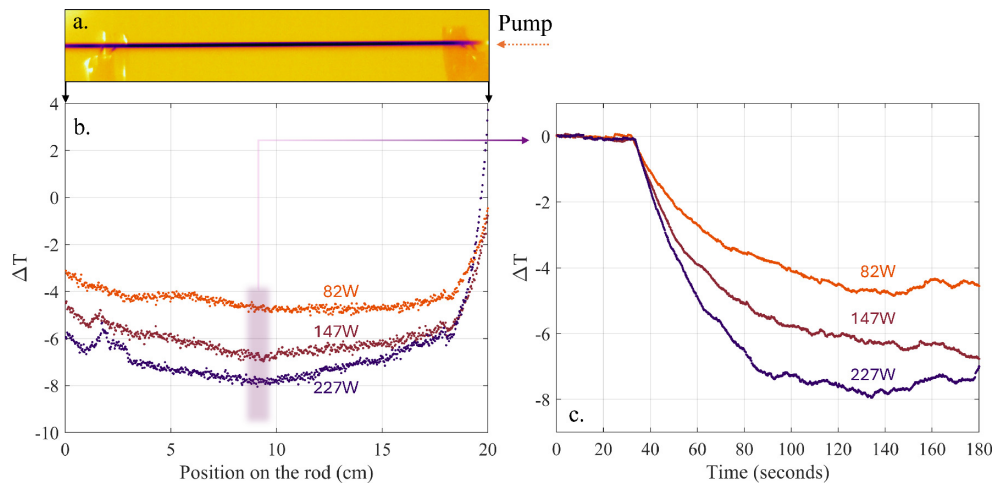
Fig. 8. a. Thermal image of the GLaA 75/25 - 25 cm rod under 1070 nm - 227 watt pumping, at t = 150 seconds. b. Temperature profile of the rod at t = 150 seconds (approximated steady state condition), for various pumping power c. Dynamic temperature evolution of the rods, for various pumping power

Figure 8 presents the ASFC results obtained from the rod, using pumping powers of 82, 147 and 227 W. Figure 8(a). presents the thermal image of the rod, for a pump power of 227 W at t = 150 seconds. Figure 8(b) shows the cooling profile along the rod, for the various pump powers. Figure 8(c) shows the dynamic evolution of temperature at x = 9.2 cm for the various pump powers. The minima established at 82, 147 and 227 W were, respectively, −4.7, −6.3 and −7.9 K with cooling time decay constants, respectively, of 31.1, 28.8 and 24.9 seconds. A localized hot spot was observed at the pump entrance, attributed to a physical defect at the core-clad interface. The silica holders did not exhibit heating with the various powers used.

4. Discussion

The present work reports the fabrication Yb-LAS glasses using the MCVD-Solution doping technique for ASFC cooling applications. The fabricated preforms were converted into bulk samples, rods, and fibers. No crystallization was observed during the thermal steps required for the various transformation. Compared to our previous results on yttrium-aluminosilicates, prepared in a similar procedure [14] the LAS matrix phase-separation effect has much slower kinetics. The non-thermally treated sample did not exhibit visible phase separation under SEM observations. Although a stronger Rayleigh scattering profile was observed in the LAS-derived fibers, it remains unclear whether this effect is attributable to phase separation occurring at a smaller scale or to refractive index heterogeneity within the material. Transmission electron microscopy observation are currently ongoing to bring light on the matter. The glass composition, showing elevated (from MCVD standards) concentrations of lanthanum, ytterbium and aluminum leads to a positive refractive index contrast of 3.10^{-2}, attaining numerical apertures of 0.31. Samples were obtained with doping concentrations up to 0.85 cationic percent, showing near-unity quantum efficiencies and background absorptions below 10 dB.km^{-1}. The radiative lifetime measured on the sample, for a 976 nm excitation, and 1030 nm emission, ranged from 0.85 to 0.87 milliseconds.. The absorption and emission cross sections also resemble to the cross sections of AS glasses, an observations that was previously made on Yb-doped LAS glasses, prepared with melt-quenching technique [18,21]. The background absorption of the sample was measured to be below 10 dB.km^{-1}, with the undoped sample exhibiting a value of 8.01 dB.km^{-1}. These results were achieved through careful selection of precursor quality, including high-purity solid dopant salts and solvents, as well as the implementation of clean preparation methods and thorough drying of the soot using both chemical and thermal treatments. Exhibiting no apparent concentration quenching, both doped samples demonstrated near-unity quantum efficiencies and showed ASFC under excitation in the range of 1030 to 1080 nm.

The first tests used samples of $12 \times 1.8 \times 1.8$ mm placed in an aluminum chamber and measured under ambient conditions. These initial measurements also included testing of an undoped LAS-series sample and a pure silica sample. Under 18 W, 1030 nm pumping, the silica sample exhibited negligible heating, estimated only at +0.1 K. In contrast, the undoped LAS sample heated by +1.2 K relative to ambient temperature. Given the background absorption of 8.01 dB · km^{-1} measured at 1030 nm, this highlights the critical importance of minimizing parasitic absorption. Moreover, while the two doped samples achieved net cooling despite similar background absorption, substantial performance gains could be achieved by further reducing impurity levels. Using a single-pass excitation setup, the GLaA 90/10 and GLaA 75/25 samples demonstrated cooling of −1.9 K and −5.5 K, respectively. In contrast, the double-pass configuration enhanced the ASFC, achieving cooling of −2.9 K and −8.2 K for the GLaA 90/10 and GLaA 75/25 samples, respectively. The additional pump absorption in the double-pass setup directly contributed to the increased ASFC. The significantly greater cooling observed in the GLaA 75/25 sample can be attributed to the nearly threefold increase in Yb concentration. Moreover, the higher Yb concentration resulted in faster cooling, as the cooling time decay

constant was reduced by half when comparing the GLaA 90/10 sample to the GLaA 75/25 sample.

The second measurement investigated the ASFC of a 25 cm long rod of the GLaA 75/25 sample. This configuration used a different excitation source operating at 1070 nm. This spectral region presents a ten-fold absorption decrease, compared to a 1030 excitation. However, the pump intensity distribution was found to be more homogeneous compared to a 1030 nm single pass scheme. The laser offered a tunable power range up to 300 W but was operated at 75% of its maximum output. Except for a heat-generating defect at the laser entrance, the results demonstrated cooling along the entire length of the rod at various pump power levels. The geometry presented a core diameter of 750 microns, smaller than the 1.6 mm core bulk sample. However, under 227 W of pump, the sample outside temperature still demonstrated cooling up to −7.9 K. The surrounding cladding still provides a higher surface area for convective heat transfer and acts as a passive thermal load. We estimated that complete removal of the cladding would enhance the cooling of the rod to −9.2 K. However, this sample geometry is likely to significantly increase reabsorption effects, as well as amplified spontaneous emissions, both of which are detrimental to ASFC. The contributions of these effects are currently under investigation.

These results demonstrate the ability of LAS-Yb glasses to demonstrate ASFC, even at doping concentrations exceeding 10^{26} ions.m^{-3}. We believe these results offer an interesting choice in the evolving context of pushing the capacities of silicate radiation-balanced fiber lasers (RBFL) to higher-power regime. In contrast, the latest ambient pressure ASFC demonstrated a −6.3 K shift for 185 W pumping at 1033 nm [24], with an Yb density roughly half of the GLaA 75/25. To the best of our knowledge, the present study represents the highest cooling reported under ambient conditions [25]. We believe these results provide a promising avenue for advancing silicate radiation-balanced fiber lasers (RBFL) toward higher power regimes. Studies suggested the use of doubly doped core-clad fiber designs that would theoretically reach an output of more than 100 W [26,27]. To accommodate larger amounts of pumping power, NA between the first doped cladding and the outer silica cladding must be high. LAS glasses have demonstrated NAs of up to 0.3, which could be further increased to 0.35 with the addition of a fluorine-doped depressed cladding. The NA of the LAS-core/LAS-clad can also be engineered for a large-mode-area architecture to enable single-mode operation. However, due to the increased complexity of these designs, the large core and cladding volumes required, and the need to maintain low background absorption, the MCVD-solution doping route presents significant technological challenges.

5. Conclusion

This study reports the fabrication of Yb-LAS glasses using the MCVD-solution doping technique. Samples were prepared with doping concentrations of up to 0.85 cationic percent, exhibiting near-unity quantum efficiencies and low background absorptions. These properties enabled cooling of centimeter-long bulk samples by up to −8.2 K from room temperature using an 18 W, 1035 nm pump. Furthermore, we demonstrate anti-Stokes fluorescence cooling in 25 cm-long rods of the material, achieving cooling of up to −7.9 K from room temperature with a 227 W, 1070 nm pump. The latter configuration presented a temperature drop throughout the entire sample length, except for a heat-generating defect at the sample entrance. To the best of our knowledge, these results represent the highest cooling values achieved in oxide glasses under ambient conditions. We hope that this study contributes to demonstrating the technological feasibility of silicates for anti-Stokes fluorescence cooling applications, while also expanding the range of compositions capable of achieving ASFC at high Yb concentrations.

Disclosures. The authors declare no conflicts of interest.

References

1. R. I. Epstein, M. I. Buchwald, B. C. Edwards, *et al.*, "Observation of laser-induced fluorescent cooling of a solid," Nature **377**(6549), 500–503 (1995).
2. G. Nemova and R. Kashyap, "Laser cooling of solids," Rep. Prog. Phys. **73**(8), 086501 (2010).
3. M. P. Hehlen, M. Sheik-Bahae, R. I. Epstein, *et al.*, "Materials for optical cryocoolers," J. Mater. Chem. C **1**(45), 7471 (2013).
4. T. R. Gosnell, "Laser cooling of a solid by 65 k starting from room temperature," Opt. Lett. **24**(15), 1041–1043 (1999).
5. J. Knall, A. Arora, M. Bernier, *et al.*, "Demonstration of anti-Stokes cooling in Yb-doped ZBLAN fibers at atmospheric pressure," Opt. Lett. **44**(9), 2338–2341 (2019).
6. Q. Xie, D. Rao, G. Yu, *et al.*, "Laser cooling by over 7 K in Yb-doped ZBLAN fibers with high-power pumping at atmospheric pressure," Opt. Lett. **48**(5), 1148–1151 (2023).
7. S. D. Melgaard, A. R. Albrecht, M. P. Hehlen, *et al.*, "Solid-state optical refrigeration to sub-100 k regime," Sci. Rep. **6**(1), 20380 (2016).
8. J. M. Knall, M. Engholm, T. Boilard, *et al.*, "Experimental demonstration of a cooled silica fiber amplifier," in *Photonic Heat Engines: Science and Applications III*, vol. 11702 (SPIE, 2021), p. 1170209.
9. E. Mobini, S. Rostami, M. Peysokhan, *et al.*, "Laser cooling of ytterbium-doped silica glass," Commun. Phys. **3**(1), 134 (2020).
10. J. M. Knall, M. Engholm, T. Boilard, *et al.*, "Radiation-balanced silica fiber amplifier," Phys. Rev. Lett. **127**(1), 013903 (2021).
11. B. Topper, A. Neumann, A. R. Albrecht, *et al.*, "Laser cooling silica: current status and future prospects," in *Photonic Heat Engines: Science and Applications* V. M. K. Kuno, P. J. Pauzauskie, and D. V. Seletskiy, eds. (SPIE, 2023), p. 3.
12. E. Balliu, B. Meehan, M. A. Cahoon, *et al.*, "High-efficiency radiation-balanced Yb-doped silica fiber laser with 200-mW output," Opt. Lett. **49**(8), 2021 (2024).
13. J. Thomas, T. Meyneng, A. Tehranchi, *et al.*, "Demonstration of laser cooling in a novel all oxide GAYY silica glass," Sci. Rep. **13**(1), 5436 (2023).
14. T. Meyneng, J. Thomas, N. Grégoire, *et al.*, "Controlled phase-separation effect for enhanced optical refrigeration in yttrium-aluminosilicate glasses," J. Mater. Chem. C **11**(23), 7619–7628 (2023).
15. P.-B. Vigneron, B. Meehan, M. A. Cahoon, *et al.*, "Anti-Stokes fluorescence cooling of nanoparticle-doped silica fibers," Opt. Lett. **47**(10), 2590 (2022).
16. M. J. Hyatt and D. E. Day, "Glass properties in the yttria-alumina-silica system," J. Am. Ceram. Soc. **70**(10), C-283–C-287 (1987).
17. J. E. Shelby, "Rare earths as major components in oxide glasses," Key Eng. Mater. **94-95**, 1–42 (1994).
18. M. J. Dejneka, B. Z. Hanson, S. G. Crigler, *et al.*, "La_2O_3-Al_2O_3-SiO_2 glasses for high-power, Yb^{3+}-doped, 980-nm fiber lasers," J. Am. Ceram. Soc. **85**(5), 1100–1106 (2002).
19. X. Wang, R. Zhang, J. Ren, *et al.*, "Mechanism of cluster dissolution of Yb-doped high-silica lanthanum aluminosilicate glass: Investigation by spectroscopic and structural characterization," J. Alloys Compd. **695**, 2339–2346 (2017).
20. A. Herrmann and C. Rüssel, "New aluminosilicate glasses as high-power laser materials," Int. J. Appl. Glass Sci. **6**(3), 210–219 (2015).
21. D. Litzkendorf, S. Grimm, K. Schuster, *et al.*, "Study of lanthanum aluminum silicate glasses for passive and active optical fibers," Int. J. Appl. Glass Sci. **3**(4), 321–331 (2012).
22. J. Thomas, T. Meyneng, A. Tehranchi, *et al.*, "Anti-Stokes cooling in highly ytterbium doped phase separated aluminium-yttrium oxide glass by 4 K," Opt. Mater. **144**, 114374 (2023).
23. B. Topper, S. Kuhn, A. Neumann, *et al.*, "Laser cooling ytterbium doped silica by 67 K from ambient temperature," Opt. Express **32**(3), 3660 (2024).
24. B. Topper, M. Peysokhan, A. R. Albrecht, *et al.*, "Laser cooling of a Yb doped silica fiber by 18 Kelvin from room temperature," Opt. Lett. **46**(22), 5707 (2021).
25. J. Ballato, P. D. Dragic, and M. J. F. Digonnet, "Prospects and challenges for all-optical thermal management of fiber lasers," J. Phys. D: Appl. Phys. **57**(16), 162001 (2024).
26. E. Mobini, M. Peysokhan, and A. Mafi, "Heat mitigation of a core/cladding Yb-doped fiber amplifier using anti-Stokes fluorescence cooling," J. Opt. Soc. Am. B **36**(8), 2167 (2019).
27. J. M. Knall and M. J. F. Digonnet, "Design of high-power radiation-balanced silica fiber lasers with a doped core and cladding," J. Lightwave Technol. **39**(8), 2497–2504 (2021).